AR expression in breast cancer CTCs associates with bone metastases

(Article begins on next page)

13 March 2024

AR Expression in breast cancer CTCs associates with bone metastases

Nicola Aceto[1,2,7], Aditya Bardia[1,2], Ben S. Wittner[1,2], Maria C. Donaldson[1], Ryan O'Keefe[1], Amanda Engstrom[1], Francesca Bersani[1,2], Yu Zheng[1,2], Valentine Comaills[1,2], Kira Niederhoffer[1], Huili Zhu[1], Olivia Mackenzie[1], Toshi Shioda[1,2], Dennis Sgroi[1,3], Ravi Kapur[5], David T. Ting[1,2], Beverly Moy[1,2], Sridhar Ramaswamy[1,2], Mehmet Toner[4,5], and Daniel A. Haber*[1,2,6] and Shyamala Maheswaran*[1,4]

[1] Massachusetts General Hospital Cancer Center, and Departments of [2] Medicine,

[3] Pathology, [4] Surgery, and [5] Center for Bioengineering in Medicine – all at Harvard

Medical School, Boston, MA 02129, USA

[6] Howard Hughes Medical Institute, Chevy Chase, MD 20815, USA

[7] Current address: Department of Biomedicine, University of Basel and University

Hospital Basel, CH-4058 Basel, Switzerland

* To whom correspondence should be addressed

Dr. Daniel A. Haber

DHABER@mgh.harvard.edu

Dr. Shyamala Maheswaran

MAHESWARAN@HELIX.MGH.HARVARD.EDU

SUMMARY

Molecular drivers underlying bone metastases in human cancer are not well understood, in part due to constraints in bone tissue sampling. Here, RNA sequencing (RNA-seq) was performed of circulating tumor cells (CTCs) isolated from blood samples of women with metastatic estrogen receptor (ER)+ breast cancer, comparing cases with progression in bone versus visceral organs. Among the activated cellular pathways in CTCs from bone-predominant breast cancer is androgen receptor (AR) signaling. AR gene expression is evident, as is its constitutively active splice variant AR-v7. AR expression within CTCs is correlated with the duration of treatment with aromatase inhibitors, suggesting that it contributes to acquired resistance to endocrine therapy. In an established breast cancer xenograft model, a bone-tropic derivative displays increased AR expression, whose genetic or pharmacologic suppression reduces metastases to bone but not to lungs. Together, these observations identify AR signaling in CTCs from women with bone-predominant ER+ breast cancer, and provide a rationale for testing androgen inhibitors in this subset of patients.

IMPLICATIONS

This study highlights a role for the androgen receptor in breast cancer bone metastasis, and suggests that therapeutic targeting of the androgen receptor may benefit patients with metastatic breast cancer.

INTRODUCTION

Metastases to bone, brain, liver and other visceral organs are primarily responsible for the lethality of breast cancer. Among these, bone metastases are the most common site of metastasis in ER-positive breast cancer(1), but the molecular characteristics that drive cancer cells to initially seed and subsequently proliferate within the bone matrix are not well understood. To date, most insight has focused on bone turnover as a key permissive factor in metastasis, with agents that suppress osteoclast activity having clinical benefit in suppressing bone-related complication of cancer(2). Less is known about the tumor-cell intrinsic properties that may direct metastasis to bone versus other organs.

In mouse models, formation of a pre-metastatic niche(3) and expression of specific cell adhesion molecules such as VCAM1, chemokines such as CXCR4, bone remodeling molecules including RANKL, OPN and Jagged1, as well as integrins associated to tumor-derived exosomes have been proposed as mediators of bone metastasis(4-7). In advanced human cancer derived from many different tissues, metastases to bone are present along with metastases within multiple visceral organs. However, prostate cancer and some ER-positive breast cancers are unique in having bone lesions as the sole site of metastatic disease, even in the presence of advanced disease(1). Thus, in addition to pathways that are intrinsic to bone, tumor-specific properties may also confer a predilection toward bone metastasis in these cancers.

CTCs are cancer cells derived from either primary or metastatic tumor deposits that are detectable as they transit through the bloodstream of patients with cancer, and may initiate new metastases at distant sites(8)⁻(9). In women who develop metastatic breast cancer several years after the removal of a primary breast tumor, CTCs are derived from metastatic lesions, and hence represent a "liquid biopsy" of multiple independent distant tumor deposits. Given the difficulty in direct sampling of bone metastases, the analysis of CTCs in this setting provides a unique opportunity to study patient-derived specimens to identify potential molecular drivers of metastasis.

METHODS

CTC capture and identification. Blood specimens for CTC analysis were obtained after informed patient consent, per IRB protocol (05-300), at the Massachusetts General Hospital and in accordance with the Declaration of Helsinki. A maximum of 20 ml of blood was drawn in EDTA vacutainers. Approximately 6-12 ml of blood was processed through the CTC-iChip within four hours from blood draw. CTC-iChips were designed and fabricated as previously described(9). Before processing, whole blood samples were exposed to biotinylated antibodies against CD45 (R&D Systems, BAM1430) and CD66b (AbD Serotec, MCA216, biotinylated in house) and then incubated with Dynabeads® MyOne™ Streptavidin T1 (Invitrogen) to achieve magnetic labeling and depletion of white blood cells(9). The CTC-enriched product was stained in solution with Alexa488-conjugated antibodies against EpCAM (Cell Signaling Technology, # 5198), Cadherin 11 (R&D Systems, FAB17901G) and HER2 (Biolegend, # 324410) to identify CTCs, and

TexasRed-conjugated antibodies against CD45 (BD Biosciences, BDB562279), CD14 (BD Biosciences, BDB562334) and CD16 (BD Biosciences, BDB562320) to identify contaminating white blood cells.

Single cell micromanipulation. The CTC-enriched product was collected in a 35mm petri dish and viewed using a Nikon Eclipse Ti inverted fluorescent microscope. Single CTCs and CTC-clusters were identified based on intact cellular morphology, Alexa488-positive staining and lack of TexasRed staining. Target cells were individually micromanipulated with a 10 μm transfer tip on an Eppendorf TransferMan® NK 2 micromanipulator and ejected into PCR tubes containing RNA protective lysis buffer (10X PCR Buffer II, 25mM MgCl2, 10% NP40, 0.1 M DTT, SUPERase-In, Rnase Inhibitor, 0.5 uM UP1 Primer, 10mM dNTP and Nuclease-free water) and immediately flash frozen in liquid nitrogen.

Single Cell RNA Amplification and Sequencing. RNA samples extracted from CTCs were thawed on ice and incubated at 70°C for 90 seconds. To generate cDNA, samples were treated with reverse transcription master mix (0.05 uL RNase inhibitor, 0.07uL T4 gene 32 protein, and 0.33uL SuperScript III Reverse Transcriptase per 1X volume) and incubated on thermocycler at 50°C for 30 minutes and 70°C for 15 minutes. To remove free primers, 1.0uL of EXOSAP mix was added to each sample, which was incubated at 37°C for 30 minutes and inactivated at 80°C for 25 minutes. Next, a 3'-poly-A tail was added to the cDNA in each sample by incubating in master mix (0.6uL 10X PCR Buffer II, 0.36uL 25mM $MgCl_2$, 0.18uL 100mM dATP, 0.3uL Terminal Transferase, 0.3uL

RNase H, and 4.26uL H_2O per 1X volume) at 37°C for 15 minutes and inactivated at 70°C for 10 minutes. A second strand cDNA was synthesized by dividing each sample into 4 (to maximize the final yield) and incubating in master mix (2.2uL 10X High Fidelity PCR Buffer, 1.76uL 2.5mM each dNTP, 0.066uL UP2 Primer at 100uM, 0.88uL 50mM $MgSO_4$, 0.44uL Platinum Taq DNA Polymerase, and 13.654uL H_2O per 1X volume) at 95°C for 3 minutes, 50°C for 2 minutes, and 72°C for 10 minutes. PCR amplification (95°C for 3 minutes, 20 cycles of 95°C for 30 seconds, 67°C for 1 minute, and 72°C for 6 minutes 6 seconds) was performed with master mix (4.1uL 10X High Fidelity PCR Buffer, 1.64uL 50mM $MgSO_4$, 4.1uL 2.5mM each dNTP, 0.82uL AUP1 Primer at 100uM, 0.82uL AUP2 Primer at 100uM, 0.82uL Platinum Taq DNA Polymerase, and 6.7uL H_2O per 1X volume). The 4 reactions of each sample were pooled and purified using the QIAGEN PCR Purification Kit (Cat. No 28106) and eluted in 50uL EB buffer. Samples were selected by testing for genes Gapdh, ActB, Ptprc (CD45), Krt8, Krt18 and Krt19 using qPCR. Each sample was again divided in 4 and a second round of PCR amplification (9 cycles of 98°C for 3 minutes, 67°C for 1 minute, and 72°C for 6 minutes 6 seconds) was performed with master mix (9uL 10X High Fidelity PCR Buffer, 3.6uL 50mM $MgSO_4$, 13.5uL 2.5mM each dNTP, 0.9uL AUP1 Primer at 100uM, 0.9uL AUP2 Primer at 100uM, 1.8uL Platinum Taq DNA Polymerase, and 59.1uL H_2O per 1X volume). Samples were pooled and purified using Agencourt AMPure XP beads and eluted in 40uL 1X low TE buffer.

Sequencing Library Construction. DNA was sheared using the Covaris S2 System, after adding 1X low TE buffer and 1.2uL shear buffer to each sample. Conditions of the

shearing program include: 6 cycles, 5°C bath temperature, 15°C bath temperature limit, 10% duty cycle, intensity of 5, 100 cycles/burst, and 60 seconds. Samples were end-polished at room temperature for 30 minutes with a master mix (40uL 5X Reaction Buffer, 8uL 10mM dNTP, 8uL End Polish Enzyme1, 10uL End Polish Enzyme2, and 14uL H$_2$O per 1X volume). DNA fragments larger than 500bp were removed with 0.5X volumes of Agencourt AMPure XP beads. Supernatant was transferred to separate tubes. To size-select 200-500bp DNA products, 0.3X volumes of beads were added and samples were washed twice with 70% EtOH. The products were eluted in 36uL low TE buffer. A dA-tail was added to each size-selected DNA by treating with master mix (10uL 5X Reaction Buffer, 1uL 10mM dATP, and 5uL A-Tailing Enzyme I per 1X volume) and incubated at 68°C for 30 minutes and cooled to room temperature. To label and distinguish each DNA sample for sequencing, barcode adaptors (5500 SOLiD 4464405) were ligated to DNA using the 5500 SOLiD Fragment Library Enzyme Module (4464413). Following barcoding, samples were purified twice using the Agencourt AMPure XP beads and eluted in 22uL low TE buffer. Following a round of PCR Amplification (95°C for 5 minutes, 12 cycles of 95°C for 15 seconds, 62°C for 15 seconds, and 70°C for 1 minute, and 70°C for 5 minutes), the libraries were purified with AMPure XP beads. Finally, to quantify the amount of ligated DNA, SOLiD Library TaqMan Quantitation Kit was used to perform qPCR. Completed barcoded libraries were then subjected to emulsion PCR with template beads preparation and sequenced on the ABI 5500XL.

Analysis of RNA Sequencing data. Determination of reads-per-million (rpm): color space reads were aligned using tophat and bowtie1 with the no-novel-juncs argument set with human genome version hg19 and transcriptome defined by the hg19 knownGene table from genome.ucsc.edu. Reads that did not align or aligned to multiple locations in the genome were discarded. The hg19 table knownToLocusLink from genome.ucsc.edu was used to map, if possible, each aligned read to the gene whose exons the read had aligned to. The reads count for each gene was the number of reads that were so mapped to that gene. This count was divided by the total number of reads that were mapped to any gene and multiplied by one million to form the reads-per-million (rpm) count. We used rpm rather than rpkm because we noted a 3' bias in the alignments. Supervised differential gene expression: samples that showed high expression of contaminant WBC markers and no expression of CTC markers at the RNA level were excluded from the analysis. The read counts for all the CTCs from a patient were summed to form a read count for that patient. Differential gene expression between groups of patients was then computed from the per-patient read counts using version 1.0.19 of the Bioconductor DESeq2 package. A gene was considered differentially expressed if its fold-change was greater than 2 and its false discovery rate (FDR) estimate as determined by DESeq2 was less than 0.25. The same procedure was also applied to the per-sample read counts. To identify pathways enriched in the differentially expressed genes we applied a hypergeometric test for each gene set in the PID subset of MSigDB v6.0. The resulting p-values were then adjusted by Benjamini/Hochberg and those with resulting FDR estimate at 0.25 or less were considered enriched. We applied the same procedure to the entire MSigDB and filtered the resulting list of enriched gene sets to find those that had " AR "

or "androgen" in their names or descriptions and then kept only those that were clearly defined by AR activity and were not down regulated in response to AR activity. Androgen receptor signature metagene: we identified seven genes (NKX3-1, PIAS1, KLK3, KLK2, TMPRSS2, MAF, and FKBP5) that were common to at least four of the six AR-related gene sets that were used in our paper. To form a single expression value for the androgen receptor signature in a sample, we took the mean of the log10(rpm) values of the seven genes for that sample. To determine whether AR expression is correlated with signature level we identified all gene sets in MSigDB that had " AR " or "androgen" in their names or descriptions. To these we added the Hieronymus signature (10). We then defined the level of the signature as described above. We then computed the Pearson p-value for correlation of each signature level with AR expression and adjusted those p-values for multiple-hypothesis testing using the Holm method. To quantify expression of AR splice variants we altered the hg19 knownGene table from UCSC by removing the AR transcripts and adding the clinically relevant transcripts AR-FL, AR-v1, AR-v3, AR-v7, and AR-v12 as defined in (11). We then proceeded as above. Reads aligning to cryptic exon 3 were considered evidence of AR-v7. Sequencing data have been deposited in the Gene Expression Omnibus database (accession no. GSE86978).

qPCR for androgen receptor target genes. qPCR for androgen receptor target genes was performed with RT2 ProfilerTM PCR Array Human Androgen Receptor Signaling Targets PCR Array (SABiosciences). MDA-MB-231-Bo cells were treated with Enzalutamide (MDV3100; SelleckChem) at 10μM or vehicle for 8 hours and then RNA

was extracted for expression analysis according to the manufacturer's instructions.

Tumorigenesis assays. All mouse experiments were carried out in compliance with institutional guidelines and upon IACUC review board approval (IACUC MGH# 2010N0000006). For tumor-derived bone metastasis studies, $2x10^6$ MDA-MB-231-Bo-GFP-Luciferase cells in 100µl PBS 50% matrigel (BD biosciences) were injected orthotopically in NSG mice. For intra-tibia injection studies, $2.5x10^5$ MDA-MB-231-Bo-GFP-Luciferase, Brx-07, Brx-61 or Brx-68 cells in 10µl PBS were injected in the tibia of NSG mice. Tumor burden was followed and quantified via noninvasive bioluminescence imaging (IVIS®, PerkinElmer) and immunohistochemical staining. Enzalutamide (VWR) was resuspended in DMSO, diluted in 0.5% carboxymethyl cellulose / 0.25% Tween-80 solution, and administered daily via oral gavage at a dosage of 10 mg/kg. All mice had a subcutaneous implant of a testosterone pellet (Innovative Research of America, # SA-151).

Immunohistochemistry. Formalin-fixed and paraffin embedded human and mouse specimens were sectioned and stained overnight at 4°C with antibodies against GFP (Cell Signaling Technology, # 2956S) and androgen receptor (Cell Signaling Technology, #5153S). All specimens were counterstained with Hematoxylin. Images of the entire tissue were taken with ScanScope (Aperio).

Immunofluorescence. Formalin-fixed samples were stained with antibodies against androgen receptor (Cell Signaling Technology, #5153S) and Ki-67 (Life Technologies, #

180191Z), plus DAPI (Life Technologies). High-resolution images were obtained with an upright fluorescence microscope (Eclipse 90i, Nikon, Melville, NY).

Immunoblotting. Total protein lysates were obtained with SDS-hot buffer (2.5% SDS, 250mM Tris-HCl pH 7.4) at $95^{o}C$ and 30µg of protein from each sample was analyzed. . Western blot was performed with antibodies against androgen receptor (Cell Signaling, #5153S) and β-Actin (BD Biosciences, # 612656).

Cell culture and reagents. MDA-MB-231-Bo cells were not authenticated and directly obtained from J. Massagué (MSKCC, New York, NY, USA) and propagated in DMEM (Life Technologies) supplemented with 10% fetal bovine serum (Life Technologies). Upon confirming the absence of Mycoplasma (MP0040, Sigma), MDA-MB-231-Bo cells were used for all experiments before passage 10 was reached. CTC-derived cell lines were established in our lab and maintained as previously described(12). The plasmid expressing GFP-Luciferase was obtained from C. Ponzetto (University of Torino, Italy). Androgen receptor TRC shRNAs were purchased from Thermo Scientific. Enzalutamide was purchased from VWR. Lentiviral packaging vectors (Addgene) were used to transfect 293T cells (ATCC) and produce lentiviral particles. Infections of target cells lines was performed overnight at a MOI=10 in growth medium containing 8 µg/ml polybrene (Thermo Scientific).

RESULTS

Thirty-two women with metastatic ER-positive breast cancer who failed multiple lines of therapy were enrolled in an IRB-approved observational study at Massachusetts General Hospital (MGH). All patients had evidence of advanced disease progression and had discontinued their therapy at the time of CTC collection. Patients with detectable CTCs (n=22) were classified dynamically based on which metastatic sites were progressing at the time of blood sampling, identifying 13 (59%) who had the appearance of new bone metastases at the time of CTC isolation (termed "Bone (+)"), versus 9 (41%) who had either no bone involvement at all or had no new bone metastases, and had disease progression at visceral or soft tissue sites (termed "Visceral (+)") (**Table S1**).

For each patient, approximately 10ml of blood was processed through the CTC-iChip(9). From the initial sample of blood (10 x 10^6 WBC/ml), the final microfluidic product contains approximately 500 residual WBCs per ml of whole blood processed, along with candidate CTCs. CTCs are identified by live staining with Alexa 488-conjugated antibodies against EpCAM, HER2 and CDH11, while WBCs are counterstained using TexasRed-conjugated antibodies against the hematopoietic markers CD45, CD16 and CD14 (**Fig. 1a**). CTCs were identified in 13 patients with Bone (+) and 9 patients with Visceral (+) disease, with a median of 3.5 CTCs per patient, leading to a total of 77 samples representing either single CTC, CTC-clusters, or in rare patients with high numbers of CTCs, pools of up to three CTCs (**Fig. 1a** and **Table S1**).

To gain insight into the signaling dynamics that occur in CTCs that are primarily derived from different metastatic sites, we generated RNA-sequencing data from all 77 CTC samples. Using a fold change greater than 2 and a false discovery rate (FDR) threshold of 0.25 for the analysis of our RNA-sequencing data, we found a total of 871 genes upregulated in CTCs from Bone (+) patients, versus 835 genes upregulated in CTCs from Visceral (+) patients (**Fig. 1b**). Analysis of these gene sets using the Pathway Interaction Database (PID) revealed differences between CTCs from patients belonging to these two groups. CTCs from patients with Visceral (+) disease displayed activation of pathways involved in cell-cell junctions, cellular signaling, epithelial-to-mesenchymal transition (EMT), platelets signaling and immune cells-like signaling (**Fig. 1c,** *left*). While CTCs from patients with Bone (+) disease also showed activation of pathways involved in EMT and immune cells-like signaling, they displayed activation of unique signaling pathways related to receptor tyrosine kinase activity (e.g. EGFR, VEGFR, PI3K and mTOR), epigenetic regulators (e.g. HDAC class 1 and class3), and androgen receptor signaling (**Fig. 1c,** *right*). Given the therapeutic opportunities presented by targeting AR and its established critical role in prostate cancer, the prototype of bone-specific metastasis, we focused our functional validation on this pathway. Further analysis of our data involving individual samples assessment (**Fig. S1a and S1b**) as well as using the Molecular Signatures Database (MSigDB) (**Fig. S1c and S1d**) confirmed the activation of AR pathway in Bone (+) CTCs.

AR gene as well as a set of AR target genes (see methods section and **Table S2**) are upregulated in CTCs from Bone (+) compared to Visceral (+) patients ($p<0.017$) (**Fig.**

2a), with AR expression levels generally correlating with activation of its target genes in multiple signatures (**Fig. S2**), suggesting that AR is not only highly transcribed, but also active in the context of breast cancer bone metastasis. In contrast to the increased AR expression levels, no change is evident in expression of either ER or the Progesterone Receptor (PR) in CTCs from Bone (+) compared to Visceral (+) patients (**Fig. S3**). AR transcripts are subject to alternative splicing, a phenomenon that has been well documented in advanced, hormone-refractory prostate cancer. Recently, a constitutively active AR splicing variant (AR-v7) has been identified as a marker of acquired resistance to the prostate cancer drugs abiraterone acetate and enzalutamide(13). AR-v7 lacks the inhibitory C-terminus ligand-binding domain of AR, making it readily detectable by RNA sequencing analysis. AR-v7 expression has also recently been identified in some cases of breast cancer(14). We identified AR-v7 sequence reads in 9/22 (41%) patients (22/77 of all CTC samples; 29%) (**Fig. 2b**). CTCs expressing AR-v7 were found in 8/13 Bone (+) versus 1/9 Visceral (+) patients (p=0.031), with the AR-v7/AR ratio varying among different patients (**Fig. 2b**). Interestingly among the entire cohort, women who had AR-positive CTCs had received a median of 725 days of treatment with an aromatase inhibitor (AI), compared with 85 days for those whose CTCs were negative for AR expression (p=0.01) (**Fig. 2c**). By analogy with the recently reported estrogen receptor (ESR1) gene mutations, which are acquired after prolonged therapy with AI and confer ligand independent activation of ER and resistance to hormonal therapy(15), this observation suggests a similar link between suppression of estrogen production and activation of androgen receptor signaling.

To extend the analysis of AR expression from CTCs to breast cancer bone metastases, we were able to analyze biopsies of metastatic deposits in the bone (n=5) and visceral organs (n=5) that had been collected from some of the patients enrolled in our study (**Table S1**). Such biopsies are infrequently obtained in the care of patients with ER-positive breast cancer. Among the limited number of samples available for analysis, we observed a trend toward increased AR expression and nuclear localization (immunohistochemistry) in bone metastases (4/5) versus visceral metastases (1/5; p=0.206) (**Fig. 3a** and **Fig. S4a,b**). AR overexpression in prostate cancer is occasionally accompanied by *AR* gene amplification, but no such gene copy alteration was evident by fluorescence *in situ* hybridization (FISH) analysis in the breast cancer metastases (**Fig. S5a,b**). We also used publicly available datasets to test clinical correlates of AR expression with clinical outcomes: in 192 cases of primary breast tumors[16], elevated levels of AR are highly correlated with the development of bone metastases (P=6.5e-07) (**Fig. 3b**). In a dataset of breast cancer biopsies taken from bone, brain or lungs from patients with metastatic breast cancer (n=29)[17], AR expression is higher in the bone lesions compared to the other sites (p=0.039) (**Fig. 3c**). A significant but much lower correlation was found between bone metastasis and ER and PR expression in the same datasets (**Fig. S6a-d**).

Finally, we used xenograft mouse models to test the functional consequences of AR expression in bone metastasis from breast cancer. While mouse models with physiological development of metastasis to bone from a primary tumor mass are limited, a bone-tropic variant has been established from the highly tumorigenic breast cancer cell

line MDA-MB-231, following serial passaging in bone lesions(18). This variant

"subclone #1833", (described here as 231-Bo) is regarded as a triple-negative breast

cancer model, however loss of ER signaling in metastatic luminal breast cancer is a well-

documented mechanism of resistance to endocrine therapy(19), and AR expression

correlates with bone metastasis independently of ER status (**Fig. S7**), thus making 231-

Bo cells a relevant model to validate our CTC data. 231-Bo cells overexpresses genes

such as interleukin 11and CTGF, and its implantation into the mammary fat pad of

immunosuppressed mice (NSG) produces a reproducible number of bone metastases,

along with numerous lung metastases(4,18). Remarkably, 231-Bo cells express 3.5-fold

higher levels of AR protein, compared with the parental 231 cells (**Fig. 4a**) and are

responsive to treatment with Enzalutamide, as shown by downregulation of AR-target

genes including AR itself, ACKR3, KLK2, KLK3, KLK4, KRT8, ORM1, ORM2, PGC,

SPDEF, STEAP4 and TMPRSS2 genes (**Fig. S8a,b**). We generated 231-Bo cells

expressing multiple shRNA constructs targeting different regions of AR transcript (**Fig.

S9**) and compared their metastatic propensity with that of 231-Bo cells expressing a

control shRNA. A testosterone pellet was implanted subcutaneously into female NSG

mice, to ensure that both ER and AR ligands were not limiting. As expected, implantation

of GFP-Luciferase tagged 231-Bo cells into the mammary fat pad resulted within 6

weeks in multiple lung metastases, as well as a small number of defined bone metastases

(a median of three foci per tibia). shRNA-mediated AR knockdown had no effect on the

primary tumor size or the overall presence of lung metastases, yet reduced the number of

bone metastases (p<0.048) (**Fig. 4b, 4c and Fig. S9, S10a-c**). We extended these findings

using parental 231-Bo-derived xenografts in mice treated with the AR inhibitor

enzalutamide. Consistent with the shRNA-knockdown, chemical suppression of AR signaling suppressed bone metastases, without affecting primary tumor size or lung metastases (p<0.009) (**Fig. 3d and Fig. S10a-c**).

DISCUSSION

By analyzing single cell RNA sequencing profiles of CTCs, we identify signaling pathways that are differentially activated in the context of bone versus visceral metastasis. Among these pathways, increased *AR* expression appears to be noteworthy in bone-predominant breast cancer, both in its occurrence as a function of aromatase inhibitor therapy, and in its possible responsiveness to anti-androgenic intervention.

Signaling pathways that are upregulated in CTCs from patients with progressing visceral metastases include those involved in cell-cell junctions stability, intracellular signaling downstream of RhoA, PTP1B and other effectors, maintenance of EMT via TGFβ receptor. In contrast, CTCs from patients with progressing bone metastases display RTK/PI3K/mTOR pathway activation, and increased expression of cytokines such as IL3 and IL6, EMT regulators such as SMAD2, HDAC epigenetic regulators, as well as AR signaling. While in this study we investigated the functional relevance of AR

in breast cancer bone metastasis, detailed analyses of multiple other pathways may reveal new organ-specific dependencies of metastatic breast cancer cells.

AR expression is well established in triple negative breast cancer (TNBC), and ongoing clinical trials are testing the effectiveness of AR inhibitors in this subtype of breast cancer(20), as well as in the other subtypes(21). These inhibitors were developed for treatment of prostate cancer, the prototype AR-driven malignancy. Physiological androgen-dependent activation of AR mediates transcription of target genes that are crucial for the development and maintenance of the prostate gland(22), a dependence that persists upon neoplastic transformation, with anti-androgen therapies as the standard of care for metastatic prostate cancer. AR and androgen synthesis genes are commonly upregulated in bone metastases from prostate cancer, compared to primary tumors(23). Androgens themselves are converted to estrogens by the enzyme aromatase, the most common therapeutic target in women with postmenopausal ER-positive breast cancer. Indeed, in women receiving aromatase inhibitor (AI) therapy for breast cancer, circulating levels of estradiol are low, while androgen levels are increased(24). It is in this setting of prolonged estrogen deprivation resulting in increased androgens, that overexpression of AR may become clinically relevant in the progression of ER-positive breast cancer, a possibility that is supported by our observed correlation between the duration of AI therapy and presence of AR-expressing CTCs. Furthermore, the detection of the constitutively activated, prostate cancer-associated AR-v7 splice variant within CTCs from breast cancer patients with bone metastases also suggests a functional role for androgen signaling.

AR expression in ER-positive breast cancer may also constitute a marker of more indolent, bone-predominant disease, rather than a direct contributor to proliferation in bone, although the suppression of bone metastases by either AR knockdown or pharmacological AR suppression in a mouse model of bone-tropic disease suggests a functional consequence of AR expression. In addition, given the use of AIs in the treatment of metastatic breast cancer, as well as their recommended prolonged use in the adjuvant setting(25), monitoring for the emergence of androgen-dependent signaling may ultimately help guide therapeutic choices. Taken all together, noninvasive sampling and single cell profiling of tumor cells from patients with distinct metastatic outcomes provides an exceptional resource to study advanced stages of progression, with the potential to impact therapeutic opportunities in the setting of refractory disease.

REFERENCES

1. Mundy GR. Metastasis to bone: causes, consequences and therapeutic opportunities. Nature reviews Cancer **2002**;2(8):584-93 doi 10.1038/nrc867.

2. Dougall WC, Holen I, Gonzalez Suarez E. Targeting RANKL in metastasis. Bonekey Rep **2014**;3:519 doi 10.1038/bonekey.2014.14.

3. Kaplan RN, Riba RD, Zacharoulis S, Bramley AH, Vincent L, Costa C, *et al.* VEGFR1-positive haematopoietic bone marrow progenitors initiate the pre-metastatic niche. Nature **2005**;438(7069):820-7 doi 10.1038/nature04186.

4. Kang Y, Siegel PM, Shu W, Drobnjak M, Kakonen SM, Cordon-Cardo C, *et al.* A multigenic program mediating breast cancer metastasis to bone. Cancer cell **2003**;3(6):537-49.

5. Muller A, Homey B, Soto H, Ge N, Catron D, Buchanan ME, *et al.* Involvement of chemokine receptors in breast cancer metastasis. Nature **2001**;410(6824):50-6 doi 10.1038/35065016.

6. Sethi N, Dai X, Winter CG, Kang Y. Tumor-derived JAGGED1 promotes osteolytic bone metastasis of breast cancer by engaging notch signaling in bone cells. Cancer cell **2011**;19(2):192-205 doi 10.1016/j.ccr.2010.12.022.

7. Hoshino A, Costa-Silva B, Shen TL, Rodrigues G, Hashimoto A, Tesic Mark M, *et al.* Tumour exosome integrins determine organotropic metastasis. Nature **2015**;527(7578):329-35 doi 10.1038/nature15756.

8. Aceto N, Bardia A, Miyamoto DT, Donaldson MC, Wittner BS, Spencer JA, *et al.* Circulating tumor cell clusters are oligoclonal precursors of breast cancer metastasis. Cell **2014**;158(5):1110-22 doi 10.1016/j.cell.2014.07.013.

9. Ozkumur E, Shah AM, Ciciliano JC, Emmink BL, Miyamoto DT, Brachtel E, *et al.* Inertial focusing for tumor antigen-dependent and -independent sorting of rare circulating tumor cells. Science translational medicine **2013**;5(179):179ra47 doi 10.1126/scitranslmed.3005616.

10. Hieronymus H, Lamb J, Ross KN, Peng XP, Clement C, Rodina A, *et al.* Gene expression signature-based chemical genomic prediction identifies a novel class of HSP90 pathway modulators. Cancer cell **2006**;10(4):321-30 doi 10.1016/j.ccr.2006.09.005.

11. Lu C, Luo J. Decoding the androgen receptor splice variants. Transl Androl Urol **2013**;2(3):178-86 doi 10.3978/j.issn.2223-4683.2013.09.08.

12. Yu M, Bardia A, Aceto N, Bersani F, Madden MW, Donaldson MC, *et al.* Cancer therapy. Ex vivo culture of circulating breast tumor cells for individualized testing of drug susceptibility. Science **2014**;345(6193):216-20 doi 10.1126/science.1253533.

13. Antonarakis ES, Lu C, Wang H, Luber B, Nakazawa M, Roeser JC, *et al.* AR-V7 and resistance to enzalutamide and abiraterone in prostate cancer. The New England journal of medicine **2014**;371(11):1028-38 doi 10.1056/NEJMoa1315815.

14. Hickey TE, Irvine CM, Dvinge H, Tarulli GA, Hanson AR, Ryan NK, *et al.* Expression of androgen receptor splice variants in clinical breast cancers. Oncotarget **2015**;6(42):44728-44 doi 10.18632/oncotarget.6296.

15. Robinson DR, Wu YM, Vats P, Su F, Lonigro RJ, Cao X, *et al.* Activating ESR1 mutations in hormone-resistant metastatic breast cancer. Nat Genet **2013**;45(12):1446-51 doi 10.1038/ng.2823.

16. Bos PD, Zhang XH, Nadal C, Shu W, Gomis RR, Nguyen DX, *et al.* Genes that mediate breast cancer metastasis to the brain. Nature **2009**;459(7249):1005-9 doi 10.1038/nature08021.

17. Zhang XH, Wang Q, Gerald W, Hudis CA, Norton L, Smid M, *et al.* Latent bone metastasis in breast cancer tied to Src-dependent survival signals. Cancer cell **2009**;16(1):67-78 doi 10.1016/j.ccr.2009.05.017.

18. Minn AJ, Gupta GP, Siegel PM, Bos PD, Shu W, Giri DD, *et al.* Genes that mediate breast cancer metastasis to lung. Nature **2005**;436(7050):518-24 doi 10.1038/nature03799.

19. Gutierrez MC, Detre S, Johnston S, Mohsin SK, Shou J, Allred DC, *et al.* Molecular changes in tamoxifen-resistant breast cancer: relationship between

estrogen receptor, HER-2, and p38 mitogen-activated protein kinase. J Clin Oncol **2005**;23(11):2469-76 doi 10.1200/JCO.2005.01.172.

20.   Arce-Salinas C, Riesco-Martinez MC, Hanna W, Bedard P, Warner E. Complete Response of Metastatic Androgen Receptor-Positive Breast Cancer to Bicalutamide: Case Report and Review of the Literature. J Clin Oncol **2016**;34(4):e21-4 doi 10.1200/JCO.2013.49.8899.

21.   O'Shaughnessy J, Campone M, Brain E, Neven P, Hayes D, Bondarenko I, *et al.* Abiraterone acetate, exemestane or the combination in postmenopausal patients with estrogen receptor-positive metastatic breast cancer. Ann Oncol **2016**;27(1):106-13 doi 10.1093/annonc/mdv487.

22.   Yeh S, Tsai MY, Xu Q, Mu XM, Lardy H, Huang KE, *et al.* Generation and characterization of androgen receptor knockout (ARKO) mice: an in vivo model for the study of androgen functions in selective tissues. Proceedings of the National Academy of Sciences of the United States of America **2002**;99(21):13498-503 doi 10.1073/pnas.212474399.

23.   Montgomery RB, Mostaghel EA, Vessella R, Hess DL, Kalhorn TF, Higano CS, *et al.* Maintenance of intratumoral androgens in metastatic prostate cancer: a mechanism for castration-resistant tumor growth. Cancer research **2008**;68(11):4447-54 doi 10.1158/0008-5472.CAN-08-0249.

24.   Dimitrakakis C, Bondy C. Androgens and the breast. Breast cancer research : BCR **2009**;11(5):212 doi 10.1186/bcr2413.

25.   Goss PE, Ingle JN, Pritchard KI, Robert NJ, Muss H, Gralow J, *et al.* Extending Aromatase-Inhibitor Adjuvant Therapy to 10 Years. N Engl J Med **2016**;375(3):209-19 doi 10.1056/NEJMoa1604700.

FIGURE LEGENDS

Fig.1. RNA sequencing of CTCs from breast cancer patients with progressive bone versus visceral metastasis. a) Schematic representation of sample processing through the CTC-iChip. Metastasis-derived CTCs were identified by staining for EpCAM, HER2 and CDH11 (green), whereas white blood cells were identified by staining for CD45, CD16 and CD14 (red). **b**) Volcano plot showing the fold change versus false discovery rate (FDR) for each individual gene in CTCs from patients with Bone(+) versus Visceral(+) metastasis. **c**) Bar graph showing all significantly enriched pathways (FDR<0.25) using the PID tool in CTCs from Bone(+) versus Visceral(+) patients. Pathways are grouped thematically into seven classes.

Fig.2. Androgen Receptor Activation in breast CTCs. a) Boxplots showing AR transcript expression in CTCs from Bone(+) versus Visceral(+) patients. Reads per million (rpm) are computed per-patient (*top*). Boxplot shows the levels of the AR signature metagene representative of AR activity (see methods section) in CTCs from patients with "Bone(+)" (*red*) versus "Visceral(+)" (*blue*) disease (*bottom*). **b**) Heatmap

showing the presence or absence of AR and AR-v7 reads, as well as the ratio between AR-v7 and AR reads, for each patient. **c**) Bar graph shows the mean number of days on aromatase inhibitor treatment for patients with AR negative versus AR positive CTCs, and for patients with AR-v7 negative versus AR-v7 positive CTCs. Error bars represent SEM. *p=0.013.

Fig. 3. Androgen Receptor Expression in metastatic breast cancer. a) Representative images of AR (brown) and hematoxylin (nuclei; blue)-stained human breast cancer bone metastasis (*left*) and soft-tissue metastasis (*right*) tissues. The bar graph (*bottom*) shows the number of AR-positive and AR-negative stains within the bone metastasis versus visceral or soft tissue metastasis. **b**) Boxplot shows AR expression levels in primary breast tumors (n=192) from patients who later developed metastasis in the bone versus other organs. **c**) Boxplot shows AR expression levels in metastatic breast cancer biopsies derived from lung, liver or bone (n=29).

Fig.4. The Androgen Receptor contributes to spontaneous bone metastasis in breast cancer. a) Immunoblot shows AR expression levels in parental, lung variant and bone variant MDA-MB-231 cells. Error bars represent SEM. n=3; *P<0.04. **b**) Schematic of the experiment to determine the propensity of AR expressing bone variant MDA-MB-231 cells to metastasize to the lung or bone (*left*). Representative images of GFP-stained primary breast tumor, lung and bone metastases (*right*) derived from the bone variant MDA-MB-231 cells inoculated into the mouse mammary gland. **c**) The bar graph shows the number of animals with bone and lung metastases in the groups harboring tumors in

which AR expression was suppressed with 2 different shRNAs versus control shRNA.

n=8; *P=0.048. **d**) The bar graph shows the number of animals with bone and lung

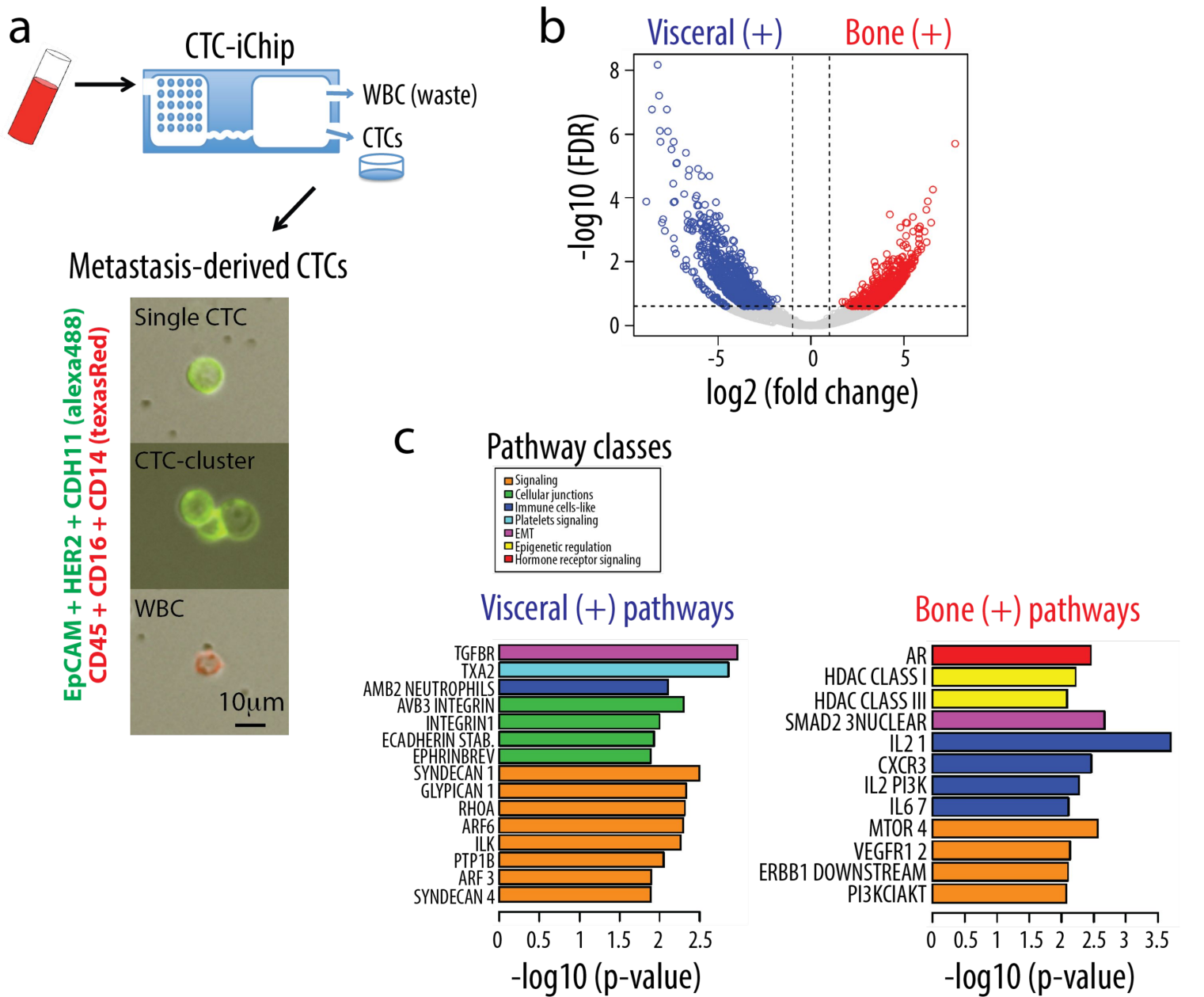metastases in the groups treated with vehicle or enzalutamide. n=8; **P<0.009 (*bottom*).

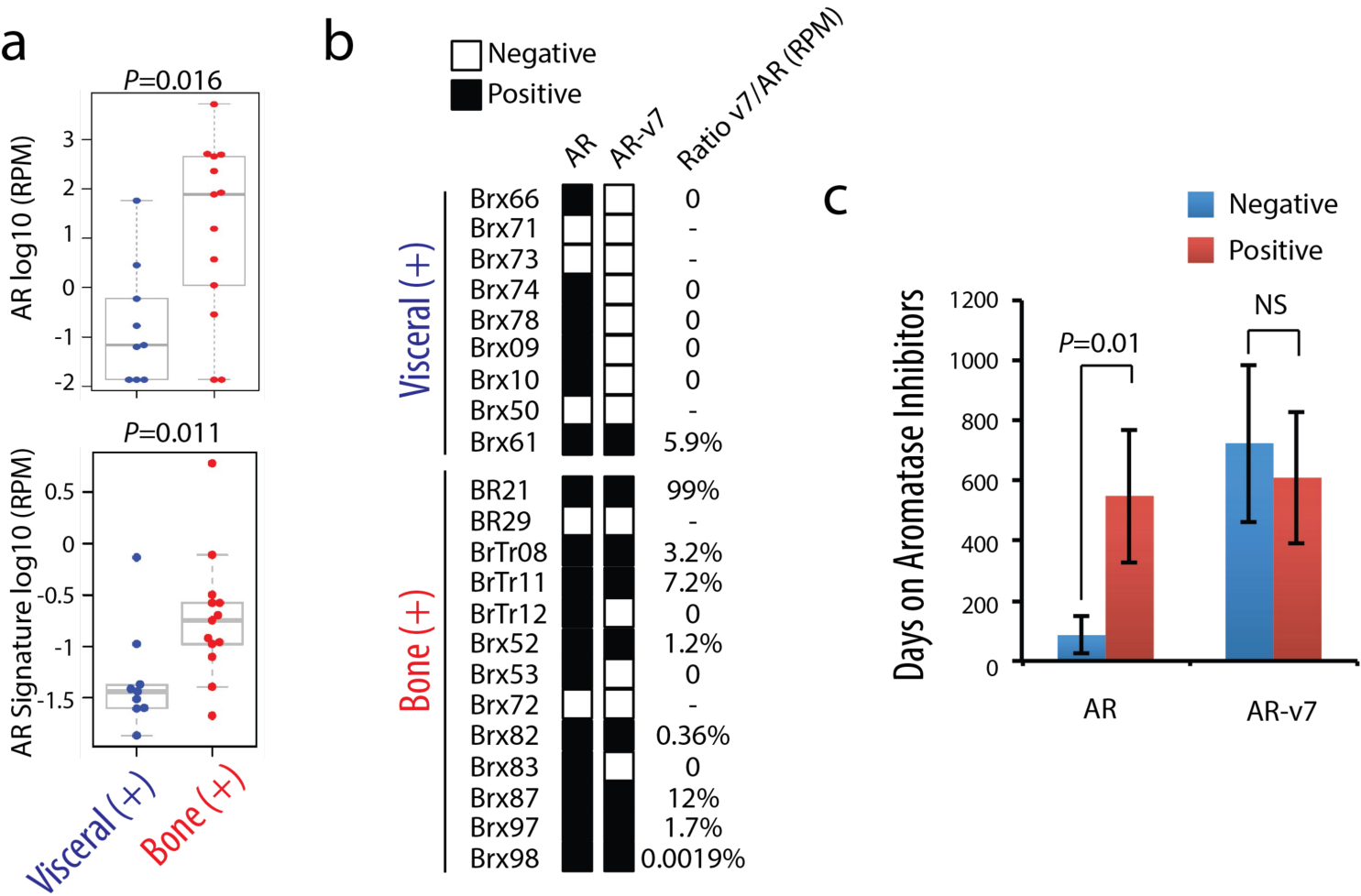FIGURE 1 Aceto et al.

a

P=0.016

AR log10 (RPM)

P=0.011

AR Signature log10 (RPM)

Visceral (+)   Bone (+)

b

☐ Negative
■ Positive

	AR	AR-v7	Ratio v7/AR (RPM)
Brx66	■	☐	0
Brx71	☐	☐	-
Brx73	☐	☐	-
Brx74	■	☐	0
Brx78	■	☐	0
Brx09	■	☐	0
Brx10	■	☐	0
Brx50	☐	☐	-
Brx61	■	■	5.9%
BR21	■	■	99%
BR29	☐	☐	-
BrTr08	■	■	3.2%
BrTr11	■	■	7.2%
BrTr12	■	☐	0
Brx52	■	■	1.2%
Brx53	■	☐	0
Brx72	■	☐	-
Brx82	■	■	0.36%
Brx83	■	☐	0
Brx87	■	■	12%
Brx97	■	■	1.7%
Brx98	■	■	0.0019%

Visceral (+): Brx66–Brx61
Bone (+): BR21–Brx98

c

■ Negative
■ Positive

Days on Aromatase Inhibitors

P=0.01   NS

AR   AR-v7
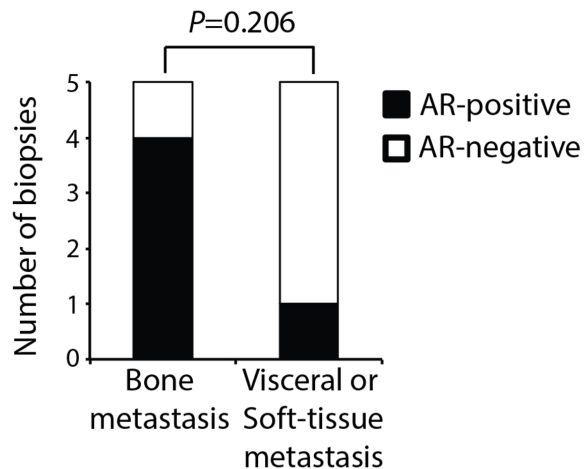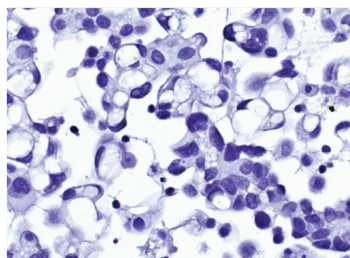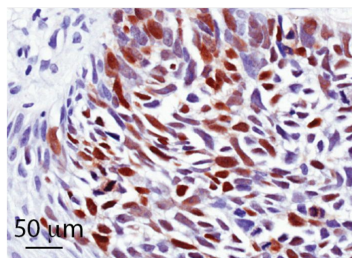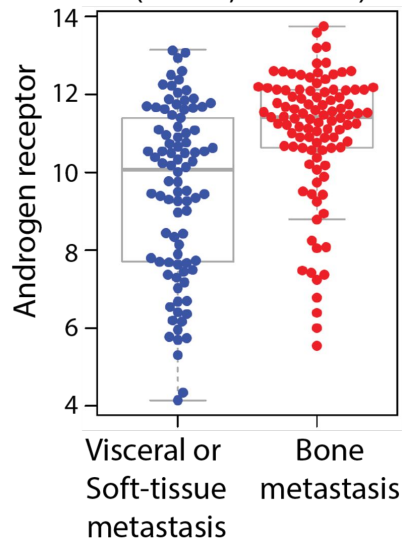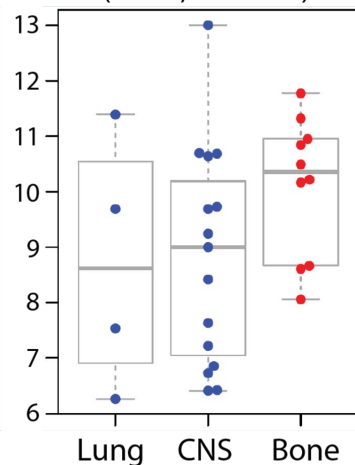
FIGURE 2 Aceto et al.

FIGURE 3 Aceto et al.

FIGURE 4 Aceto et al.